The Astrophysical Journal Letters, 789:L37 (5pp), 2014 July 10 doi:10.1088/2041-8205/789/2/L37


# PAIR-DOMINATED GeV–OPTICAL FLASH IN GRB 130427A

Indrek Vurm[1,2], Romain Hascoët[1], and Andrei M. Beloborodov[1]
[1] Physics Department and Columbia Astrophysics Laboratory, Columbia University,
538 West 120th Street, New York, NY 10027, USA; indrek.vurm@gmail.com
[2] Tartu Observatory, Tõravere 61602, Tartumaa, Estonia
*Received 2014 February 11; accepted 2014 May 9; published 2014 June 26*

## ABSTRACT

We show that the light curve of the double GeV+optical flash in GRB 130427A is consistent with radiation from the blast wave in a wind-type medium with density parameter $A = \rho r^2 \sim 5 \times 10^{10}$ g cm$^{-1}$. The peak of the flash is emitted by copious $e^{\pm}$ pairs created and heated in the blast wave; our first-principle calculation determines the pair-loading factor and temperature of the shocked plasma. Using detailed radiative transfer simulations, we reconstruct the observed double flash. The optical flash is dominated by synchrotron emission from the thermal plasma behind the forward shock, and the GeV flash is produced via inverse Compton (IC) scattering by the same plasma. The seed photons for IC scattering are dominated by the prompt MeV radiation during the first tens of seconds, and by the optical to X-ray afterglow thereafter. IC cooling of the thermal plasma behind the forward shock reproduces all GeV data from a few seconds to ∼1 day. We find that the blast wave Lorentz factor at the peak of the flash is $\Gamma \approx 200$, and the forward shock magnetization is $\varepsilon_B \sim 2 \times 10^{-4}$. An additional source is required by the data in the optical and X-ray bands at times $>10^2$ s; we speculate that this additional source may be a long-lived reverse shock in the explosion ejecta.

*Key words:* gamma-ray burst: general – plasmas – radiation mechanisms: non-thermal – radiative transfer – scattering

*Online-only material:* color figures

## 1. INTRODUCTION

GRB 130427A was an exceptionally bright gamma-ray burst (GRB) due to its relative proximity (cosmological redshift $z = 0.34$; Levan et al. 2013) and high luminosity reaching $L_{\rm MeV} \sim 3 \times 10^{53}\,{\rm erg\,s^{-1}}$ in the MeV band (Ackermann et al. 2014, hereafter A14; Golenetskii et al. 2013). The burst was accompanied by a GeV flash with peak luminosity $L_{\rm GeV} \sim 10^{51}\,{\rm erg\,s^{-1}}$ (A14) and an optical flash with peak luminosity $L_{\rm O} \sim 10^{49}\,{\rm erg\,s^{-1}}$ (Vestrand et al. 2014). It is the first GRB observed at early times $t_{\rm obs} < 100$ s by both optical and GeV telescopes.

Remarkably, the optical and GeV flashes peaked at approximately the same time $t_{\rm obs} \sim 15$ s, and both showed a smooth decay after the peak; the optical flux decay $F_\nu \propto t^{-1.67}$ was steeper than that in the GeV band. Such double (optical+GeV) flashes were predicted to result from copious $e^{\pm}$ pair creation in the blast wave of the GRB explosion (Beloborodov et al. 2014, hereafter B14). In this Letter, we apply this model to GRB 130427A.

In our model, the GeV emission is produced by inverse Compton (IC) cooling of the blast wave (see also Beloborodov 2005; Fan et al. 2005). The observed spectrum extends to at least ∼100 GeV, with a 95 GeV photon detected at 243 s and a 32 GeV photon at 34 ks. Such high-energy photons cannot be produced by synchrotron emission (de Jager & Harding 1992; Piran & Nakar 2010; A14; Fan et al. 2013), which makes a strong case for their IC origin.

We calculate the synchrotron and IC cooling of the plasma heated in the forward shock of the explosion using the Monte Carlo radiative transfer code developed in B14. The code self-consistently solves the coupled problem of radiative transfer, pair creation, and blast wave dynamics. The original version of the code included only the prompt radiation as a source of target photons for IC scatterings; here we also include the optical to X-ray afterglow radiation, which dominates seed photons for IC scattering at late times. The prompt and afterglow radiation densities used in our calculations are taken from observations.

## 2. GeV FLASH

### 2.1. Pair-dominated Peak

The external medium ahead of the blast wave is exposed to the prompt GRB radiation, which pre-accelerates the medium and loads it with copious $e^{\pm}$ pairs (Thompson & Madau 2000; Beloborodov 2002). Bright bursts $e^{\pm}$ enrich the external medium by a factor $Z_\pm \gg 1$ at radii $R < 10^{17}$ cm. B14 showed that this effect leads to a bright GeV+optical flash. The forward shock heats the pair-enriched medium to the thermal Lorentz factor given by

$$\gamma_{\rm inj} \approx \frac{\Gamma}{\gamma_{\rm pre}(1+\beta_{\rm pre})}\left(1+\varepsilon_e\frac{\mu_e m_p}{Z_\pm m_e}\right), \quad (1)$$

where $\Gamma$ is the blast wave Lorentz factor, $\gamma_{\rm pre}$ is the pre-acceleration Lorentz factor of the $e^{\pm}$-loaded medium ahead of the blast wave, $\beta_{\rm pre} = (1 - 1/\gamma_{\rm pre}^2)^{1/2}$, $\mu_e$ is the ion mass per proton in units of $m_p$ ($\mu_e = 1$ for hydrogen and 2 for heavier elements), and $\varepsilon_e$ is the fraction of shocked ion energy transferred to leptons; B14 showed that at early times $\varepsilon_e \approx 1$. In our numerical model presented below we assume $\varepsilon_e = 1$ as long as $Z_\pm > 500$; at later times we take $\varepsilon_e = 0.3$, as suggested by plasma shock simulations (Sironi & Spitkovsky 2011).

The pair-loading factor $Z_\pm$ steeply decreases at $R \gtrsim 10^{16}$ cm and hence $\gamma_{\rm inj}$ grows (Figure 1). This implies a steep rise in the energy of the IC photons, $E_{\rm IC} \sim \gamma_{\rm inj}^2 E_t$, where $E_t$ are the energies of the seed/target photons. As long as the blast wave overlaps with the prompt radiation, the seed radiation is dominated by

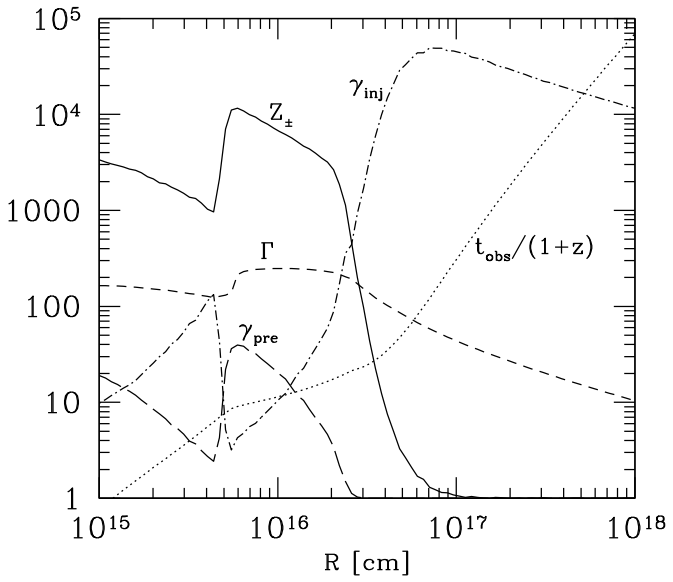


**Figure 1.** Various quantities at the forward shock as a function of radius: pair-loading factor $Z_\pm$ (solid line), pre-acceleration Lorentz factor $\gamma_{\rm pre}$ (long-dashed line), blast wave Lorentz factor $\Gamma$ (short-dashed line), and electron injection Lorentz factor $\gamma_{\rm inj}$ (dash-dotted line). The shapes of $Z_\pm(R)$ and $\gamma_{\rm pre}(R)$ are controlled by the details of the observed prompt emission and obtained numerically, as explained in B14. Dotted curve shows $t_{\rm obs}/(1+z)$ (in seconds), where $t_{\rm obs}$ is the arrival time of photons emitted at angle $\theta = \Gamma^{-1}$.

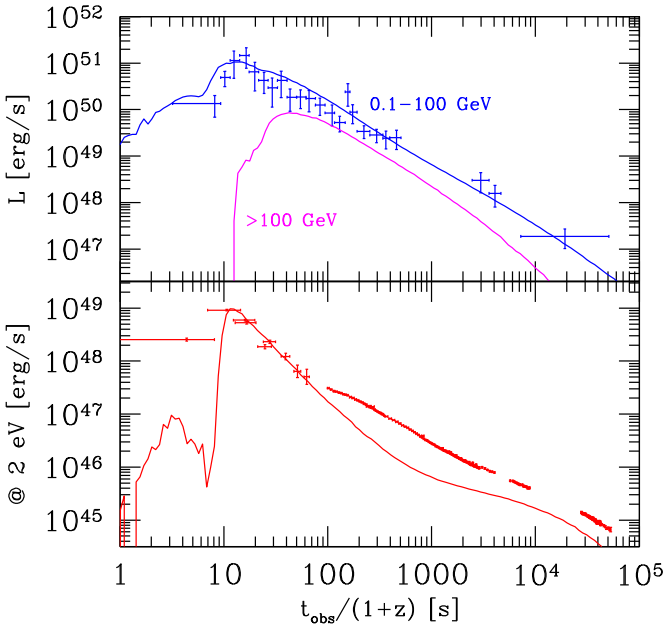


**Figure 2.** Simulated light curves and data for the GeV (upper panel) and optical (lower panel) flashes in GRB 130427A. Parameters: wind density $A = 5\times10^{10}$ g cm$^{-1}$, ejecta kinetic energy $\mathcal{E}_{\rm kin} = 2.5\times10^{53}$ erg, forward shock magnetization $\varepsilon_{\rm B} = 2\times10^{-4}$, Lorentz factor of the unshocked jet $\Gamma_{\rm ej} = 350$, ion mass per proton $\mu_e = 2$ (in units of $m_p$). The GeV data is from A14, the optical data is from Vestrand et al. (2014) and Perley et al. (2014).

(A color version of this figure is available in the online journal.)

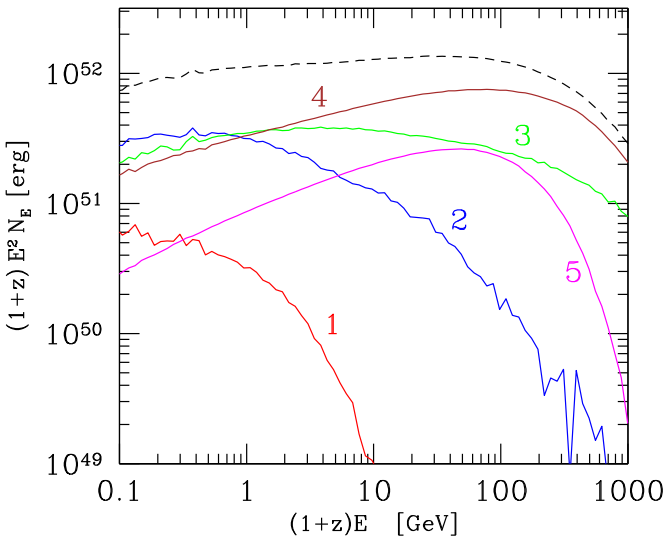


**Figure 3.** High-energy radiation spectrum in five time intervals: 0–10 s (1, red), 10–30 s (2, blue), 30–100 s (3, green), 100–3000 s (4, brown), and 3000–80000 s (5, magenta). The black dashed line shows the total fluence spectrum.

(A color version of this figure is available in the online journal.)

the prompt photons with $E_t \lesssim 1$ MeV. The onset (and peak) of the GeV flash marks the moment when $E_{\rm IC}$ reaches the GeV band. This occurs when $\gamma_{\rm inj}$ exceeds ~30.

The condition $\gamma_{\rm inj} \sim 30$ together with the observed peak time $T_p$ determines the radius and Lorentz factor of the blast wave (B14). For GRB 130427A we find

$$R_p = 1.6\times10^{16}\left(\frac{\mathcal{E}_{\rm GRB}}{8\times10^{53}\,{\rm erg}}\right)^{1/2}{\rm cm}, \quad (2)$$

$$\Gamma(R_p) \approx 150\left(\frac{\mathcal{E}_{\rm GRB}}{8\times10^{53}\,{\rm erg}}\right)^{1/4}\left(\frac{T_p}{15\,{\rm s}}\right)^{-1/2}. \quad (3)$$

Here $\mathcal{E}_{\rm GRB}$ is normalized to the energy of the main prompt MeV episode (Golenetskii et al. 2013) and we have used $z = 0.34$ (Levan et al. 2013).

Assuming that the external medium is a wind from the massive progenitor of the burst, the expected number of GeV photons in the peak of the flash is (B14)

$$N_{\rm GeV} \sim 8\times10^{51}\,Z_\pm\,\frac{A_{11}R_{16}}{\mu_e}\,\mathcal{M}, \quad (4)$$

where $A = \rho R^2 =$ constant is the wind density parameter, and $\mathcal{M} \sim$ 5–10 is the multiplicity of photons emitted above 100 MeV by a single fast-cooling electron. The pair-loading factor $Z_\pm$ steeply drops from $10^3$ to $10^2$ at $R \approx R_p$ (Figure 1). Comparing Equation (4) with the observed $N_{\rm GeV} \sim 5\times10^{54}$ (A14; Fan et al. 2013), we conclude that $A = 10^{10}$–$10^{11}$ g cm$^{-1}$ is required. Our detailed transfer simulations show that $A \sim 5\times10^{10}$ g cm$^{-1}$ gives a GeV flash that is close to the observed one.

The simulated GeV light curve is shown in the upper panel of Figure 2; the corresponding high-energy spectra at five time intervals are plotted in Figure 3. The emission above 100 MeV is initially soft, but quickly hardens as $\gamma_{\rm inj}$ exceeds 30 and then the spectrum remains roughly flat in $\nu F_\nu$. The maximal photon energy, $E_{\rm IC,max} = m_e c^2\Gamma\gamma_{\rm inj}(1+z)^{-1}$, evolves to the TeV range within a few dynamical times as $Z_\pm$ drops.

### 2.2. Blast Wave Deceleration

Our model for the GeV flash gives the parameters $A$, $R_p$, and $\Gamma(R_p)$, and implies the explosion energy

$$\mathcal{E}_{\rm kin} \approx 2.5\times10^{53}\,{\rm erg}. \quad (5)$$

It implies a high radiative efficiency of the prompt emission, $\mathcal{E}_{\rm MeV}/(\mathcal{E}_{\rm kin}+\mathcal{E}_{\rm MeV})\approx 0.8$. If the prompt emission is considered as a proxy for the ejecta power, one infers that most of the ejecta kinetic energy is contained in a shell of material about 15 light-seconds thick. The (formal) deceleration radius of the blast wave is

$$R_{\rm dec}=5\times10^{15}\,\frac{\mathcal{E}_{\rm kin}}{2.5\times10^{53}\,{\rm erg}}\times\left(\frac{A}{5\times10^{10}\,{\rm g\,cm^{-1}}}\right)^{-1}\left(\frac{\Gamma}{200}\right)^{-2}{\rm cm}. \quad (6)$$

The corresponding timescale $R_{\rm dec}/(2c\Gamma^2)$ is shorter than the duration of the prompt emission. Therefore the reverse shock in this explosion must be relativistic; it crosses the shell in approximately the same time as it takes the main prompt episode to completely overtake the forward shock. The reverse shock crossing marks the time when the bulk of the jet kinetic energy has been transferred to the blast wave. At this point the blast wave is still radiatively efficient (as the pair-loading factor $Z_\pm$ is still high); the explosion loses a substantial fraction of its initial energy during the first 20–100 s. This results in the steep decline of $\Gamma(R)$ at $R\sim(2\text{–}5)\times10^{16}$ cm (Figure 1). At $t\sim100$ s the blast wave approaches the adiabatic self-similar regime with $\Gamma\propto[\mathcal{E}_{\rm kin}/(At)]^{1/4}$ and $R\propto(\mathcal{E}_{\rm kin}t/A)^{1/2}$.

### 2.3. Transition to Synchrotron-self-Compton Cooling

The prompt radiation decouples from the forward shock at ∼30 s and does not contribute to IC cooling at later times. Then the blast wave is mainly cooled by IC scattering of the afterglow radiation, which is produced by the blast wave itself via synchrotron emission (see also Liu et al. 2013; Tam et al. 2013). Remarkably, the transition to the "synchrotron-self-Compton" (SSC) phase is smooth, with no easily recognizable feature in the GeV light curve (Figure 2). The main reason for this is that the electrons at this stage are still in the fast-cooling regime, which renders their IC emission insensitive to the target photon luminosity.

At the beginning of the SSC phase, $\gamma_{\rm inj}$ is already high and the IC scattering is dominated by low-energy photons, below the Klein–Nishina energy:

$$E_{\rm KN}\approx\frac{\Gamma m_ec^2}{\gamma_{\rm inj}(1+z)}=1\,\varepsilon_{e,-1}^{-1}\,{\rm keV}, \quad (7)$$

where we have used Equation (1) with $Z_\pm=1$ and $\gamma_{\rm pre}=1$, as pair creation is weak at late times. Equation (7) along with $E_{\rm IC}\propto E_t$ implies that the energies of target photons upscattered to the Large Area Telescope (LAT) band range from optical to soft X-rays. We approximate the spectral luminosity of the target (afterglow) radiation as

$$L_E=L_E^0\left(\frac{E_t}{1\,{\rm keV}}\right)^{-\alpha}t_3^{-\beta}, \quad (8)$$

where $t=t_{\rm obs}/(1+z)$. We use $L_E^0=3\times10^{56}\,{\rm s^{-1}}$, $\alpha=0.55$ for the optical to X-ray spectral index, and $\beta=1.1$ for the temporal index (e.g., Perley et al. 2014).

The IC cooling time of the thermal plasma behind the forward shock becomes longer than the dynamical time at $t\sim10^4$ s. Our numerical calculations show that the transition to the slow-cooling regime is very gradual with no easily identifiable spectral or temporal signature in the GeV emission (Figure 2).

The decay slope of the high-energy light curve cannot be described by a simple analytical model. Naively, in the fast-cooling stage one would expect $E_{\rm IC}L_E(E_{\rm IC})\propto\varepsilon_eL_{\rm diss}(E_{\rm IC}/E_{\rm IC,max})^{-\alpha+1}$, where $L_{\rm diss}=8\pi c^3A\Gamma^4$ is the total luminosity dissipated at the shock, yielding $E_{\rm IC}L_E(E_{\rm IC})\propto\varepsilon_e^{0.55}\mathcal{E}_{\rm kin}^{0.78}A^{0.22}E_{\rm IC}^{0.45}t^{-0.78}$. Similarly, in the slow-cooling phase $E_{\rm IC}L_E(E_{\rm IC})\propto\tau_{\rm T}\gamma_{\rm inj}^2E_tL_E(E_t)\propto\varepsilon_e^{1.1}\mathcal{E}_{\rm kin}^{-0.23}A^{1.2}E_{\rm IC}^{0.45}t^{-1.9}$. The simulated light curve is inconsistent with either regime and decays approximately as $t^{-1.2}$ up to $\sim10^4$ s.

This behavior results from a few effects. In the fast-cooling phase the temporal decay is steeper than the naive prediction due to the contribution from secondary pairs produced by the partial absorption of the GeV flash; this effect declines with time and becomes negligible at a few 100 s. The decreasing pair loading (up to ∼100 s) also somewhat steepens the light curve. Furthermore, the large-angle GeV radiation from the main peak affects the observed light curve after the peak. The gradual transition to the slow-cooling regime around $\sim10^4$ s results in a broad bump in the light curve as electrons start accumulating at $\gamma_{\rm inj}$; the asymptotic slow-cooling regime is only approached at $t\gtrsim1$ day.

The maximum energy of IC photons produced by the thermal electron population, $E_{\rm IC,max}=270\,\varepsilon_{e,-1}\mathcal{E}_{\rm kin,54}^{1/2}A_{11}^{-1/2}t_3^{-1/2}$ GeV, can accommodate the observed multi-GeV photons at late times, in particular the 32 GeV photon observed at 34 ks.

### 2.4. TeV Emission

The relative proximity and high luminosity of GRB 130427A makes it an interesting target for very high energy (VHE) observations. Our model predicts emission of photons of energies ∼1 TeV. The simulated VHE light curve above 100 GeV is shown in the top panel of Figure 2 (magenta line). The luminosity above 100 GeV reaches the peak of $\sim8\times10^{49}$ erg s$^{-1}$ during the first minute, and most of the VHE fluence should be received in ∼1000 s. Such flashes are detectable with current Cerenkov telescopes. To our knowledge no rapid VHE follow-up was performed for GRB 130427A by presently operating observatories. VERITAS obtained an upper limit at ∼1 day, which indicates a (temporal or spectral) break when compared with the extrapolation of the earlier LAT observation below 100 GeV (J. McEnery 2013, private communication). This is consistent with our model, as the predicted VHE emission from the thermal electrons behind the shock cuts off at about 50 ks, when the characteristic IC photon energy falls below 100 GeV.

## 3. OPTICAL FLASH

The optical flash is produced by synchrotron emission from the same thermal electrons injected at the forward shock that give rise to the GeV emission (B14). The mechanism of the delayed onset, peak and early decay is also analogous. The bright optical flash occurs when the synchrotron emission reaches the optical band as the electron injection Lorentz factor increases, i.e., when $\gamma_{\rm inj}=\gamma_{\rm opt}$, where

$$\gamma_{\rm opt}=\left(\frac{5E}{\Gamma h\nu_B}\right)^{1/2}\approx500\,(\varepsilon_{B,-3}A_{11})^{-1/4}\,R_{16}^{1/2}\,\Gamma_2^{-1}\times[\gamma_{\rm pre}(1+\beta_{\rm pre})]^{1/4}\left(\frac{E}{2\,{\rm eV}}\right)^{1/2}, \quad (9)$$

and $\nu_B=eB/(2\pi m_ec)$ is the cyclotron frequency.

The energetic pairs behind the shock are in the fast-cooling regime at the peak of the flash. As the electron/positron cools, most of the optical radiation is emitted when its Lorentz factor $\gamma \sim \gamma_{\rm opt}$. The approximate optical luminosity is given by (B14)

$$L_{\rm O} \approx Z_{\pm} \frac{dN_{\rm p}}{dR} \frac{dR}{dt} \frac{m_e c^2 \gamma_{\rm opt} \Gamma}{2} f_{\rm syn}, \quad (10)$$

where the factor $f_{\rm syn} \approx U_{\rm B}/U_{\rm rad}$ accounts for the fraction of energy radiated as synchrotron emission. The observed optical luminosity near the peak, $\sim 10^{49}$ erg s$^{-1}$, requires $\varepsilon_{\rm B} \sim 10^{-4}$–$10^{-3}$.

The theoretical optical light curve at 2 eV is plotted in the lower panel of Figure 2. Compared to the GeV flash, the onset is slightly delayed, because the threshold $\gamma_{\rm inj}$ for producing synchrotron optical radiation is somewhat higher than that for producing IC GeV radiation. The decay of the optical flash is controlled by the declining pair-loading factor $Z_{\pm}$ and is consistent with the observed light curve up to $\sim$100 s. At later times synchrotron emission from nonthermal electrons must take over, which is not included in the model shown in Figure 2.

## 4. DISCUSSION

The observed GeV flash in GRB 130427A can be explained as IC emission from the thermal plasma behind the blast wave in a wind medium, once the pair loading of the blast wave is correctly taken into account. The same model reproduced the GeV flash in GRB 080916C (B14). The exceptional LAT data for GRB 130427A, which extends to $\sim$1 day, made it possible to test the model at longer times, when the seed photons for IC scattering change from the prompt radiation to the afterglow. We found that this transition leaves no sharp features and is consistent with the entire observed light curve of GeV emission.

The hot $e^{\pm}$ plasma in the blast wave must also emit synchrotron radiation, in particular in the optical band. The predicted optical light curve is very close to the optical flash observed during the first 100 s (Figure 2). This provides further support to the proposed model.

Figure 2, the main result of this Letter, shows only emission from the *thermal* plasma behind the forward shock, which is a robust consequence of shock heating and is straightforward to model from first principles. We also performed a simulation including a nonthermal population of leptons in the forward shock, with an injection spectrum $dN_{\rm inj}/d\gamma \propto \gamma^{-p}$ (with $p = 2.2$) carrying a fraction $\varepsilon_{\rm nth} = 0.1$ of the shock energy. We found that the additional synchrotron and IC radiation produced by this nonthermal component weakly affects the predicted GeV+optical flash. We conclude that the thermal postshock plasma dominates the flash, at least in the region of parameter space explored by our simulations. A higher $\varepsilon_{\rm nth}$ and a flat electron spectrum $p \approx 2$ would make the contribution from nonthermal particles more significant, especially before the peak of the flash, making the rise toward the peak less sharp. Detailed models with thermal+nonthermal shocked plasma are deferred to a future paper.

After the peak, the synchrotron frequency of the thermal electrons heated by the forward shock $\nu_{\rm syn,th}$ remains above the optical band until $\sim 10^4$ s. In this situation, the addition of nonthermal electrons with $\gamma > \gamma_{\rm inj}$ does not significantly increase the optical emission from the forward shock. The additional (nonthermal) contribution to the optical afterglow observed at $10^2$–$10^4$ s should be produced by a different source, most likely a long-lived reverse shock (Uhm & Beloborodov 2007; Genet et al. 2007). This agrees with the suggestion of previous works on GRB 130427A (Panaitescu et al. 2013; Laskar et al. 2013; Perley et al. 2014).

Our flash model requires the wind density parameter $A \sim 5 \times 10^{10}$ g cm$^{-1}$. It is much higher (and more typical of Wolf–Rayet stars) than previously inferred from nonthermal afterglow modeling at $t > 10$ minutes (Panaitescu et al. 2013; Laskar et al. 2013; Perley et al. 2014). A constraint on $A$ from the late afterglow comes from the following consideration. When the characteristic synchrotron frequency of the forward shock crosses the optical band (which happens at $t \sim 10^4$ s in our model) its predicted optical flux is $F_\nu \sim 2\, A_{11} (\varepsilon_e/0.3)^{-2} (\mu_e/2)^{-3}\, t_4$ mJy. It should not exceed the observed flux of 2 mJy, a condition satisfied by our model. Models assuming $\mu_e = 1$ (hydrogen) and $\varepsilon_e = 0.1$ require smaller $A$, in agreement with Panaitescu et al. (2013). One should also keep in mind that the wind density profile may deviate from $R^{-2}$, i.e., the effective $A$ may change in the late afterglow. Yet we find no conflict between $A \sim 5 \times 10^{10}$ g cm$^{-1}$ and radio data at $t > 1$ day; the blast wave can produce radio emission without significant self-absorption in the forward or reverse shock.

Our model implies a high radiative efficiency of the blast wave at early times, when pair loading is strong. During the first few 100 s the blast wave energy $\mathcal{E}_{\rm kin}$ drops from $2.5 \times 10^{53}$ erg to $\sim 10^{53}$ erg. We expect that in a more detailed model a long-lived reverse shock will add energy to the blast wave and keep $\mathcal{E}_{\rm kin}$ from falling to such low values. A few lines of evidence suggest this energy injection. First, this would help to explain the high X-ray luminosity. Without additional energy the power dissipated in the forward shock is low:

$$L_{\rm diss} = \mathcal{E}_{\rm kin}/4t = 2.5 \times 10^{49}\, \mathcal{E}_{\rm kin,53}\, t_3^{-1} \text{ erg s}^{-1}. \quad (11)$$

It is only a factor of nine higher than the observed 0.3–10 keV luminosity at $t \gtrsim 10^3$ s, which would require a very high efficiency of X-ray emission. Secondly, the observed X-ray spectral index indicates that the (nonthermal) electrons are radiating X-rays in the slow-cooling regime already at $\sim$1000 s. At these early times, electrons are mainly cooled by IC scattering (not synchrotron) and the cooling frequency $\nu_{\rm syn,c}$ is very sensitive to the blast wave energy, $\nu_{\rm syn,c} \propto \varepsilon_{\rm B}^{1/2} \mathcal{E}_{\rm kin}^{p} t^{q}$, where $p = (4 + \alpha)/2\alpha \approx 4.1$, $q = (4\beta - 3\alpha)/2\alpha \approx 2.5$, and $\alpha$, $\beta$ are the afterglow spectral and temporal indices defined in Equation (8). Energy injection via the reverse shock would help to keep $\nu_{\rm syn,c}$ above the X-ray band. We find that supplying $\mathcal{E}_{\rm kin} \sim 10^{54}$ erg by $t \sim 1000$ s may be sufficient to explain the slow-cooling regime in the X-ray band. This can be accomplished by a tail of the GRB jet with $\Gamma_{\rm tail} \approx 50$–$100$ carrying energy comparable to the jet head.

The increased $\mathcal{E}_{\rm kin}$ will boost the optical luminosity, which can overshoot the observed afterglow, in particular when $\nu_{\rm syn,th}$ crosses the optical band at $t \sim 10^4$ s. This problem could be resolved if $\varepsilon_{\rm B}$ is reduced by a factor of $\sim$30 by that time. It is not unreasonable to assume that $\varepsilon_{\rm B}$ evolves, as physical conditions change in the expanding blast wave; e.g., the pair loading is quickly decreasing. Another factor that can reduce $\varepsilon_{\rm B}$ is the increasing cooling length of the shock-heated plasma. Note that $\varepsilon_{\rm B}$ describes the *average* value of the magnetic field in the emission region and depends on how quickly the field decays downstream of the shock (e.g., Lemoine et al. 2013).

The reduction of $\varepsilon_B$ in the late afterglow phase is also suggested by the high value of the cooling frequency, $\nu_{syn,c}$, inferred from observations by *NuSTAR* at $t \sim 1$ day. *NuSTAR* identified a break at ∼100 keV in the afterglow spectrum, which was interpreted as a cooling break (Kouveliotou et al. 2013). With no evolution of $\varepsilon_B$, our model would predict the break at a few keV while a reduction of $\varepsilon_B$ by a factor of ∼10 between $10^2$ and $10^5$ s would move the cooling break to ∼100 keV (note that cooling at 1 day is dominated by synchrotron emission, not by IC scattering, and therefore $\nu_{syn,c} \propto \varepsilon_B^{-3/2}\mathcal{E}_{kin}^{1/2}t^{1/2}$).

Detailed modeling of the nonthermal optical and X-ray emission from the forward and long-lived reverse shocks is an involved problem, which we defer to a future work. It should not, however, change the results of the present Letter. We emphasize that both the optical flash and the *entire* GeV light curve are insensitive to the details of energy injection and the evolution of $\varepsilon_B$. The same is true for our estimate of the wind density parameter $A$.

This work was supported by NSF grant AST-1008334 and NASA Fermi Cycle 6 grant NNX 13AP246.

## REFERENCES

Ackermann, M., Ajello, M., Asano, K., et al. 2014, Sci, 343, 42
Beloborodov, A. M. 2002, ApJ, 565, 808
Beloborodov, A. M. 2005, ApJL, 618, L13
Beloborodov, A. M., Hascoet, R., & Vurm, I. 2014, ApJ, 788, 36
de Jager, O. C., & Harding, A. K. 1992, ApJ, 396, 161
Fan, Y.-Z., Tam, P. H. T., Zhang, F.-W., et al. 2013, ApJ, 776, 95
Fan, Y. Z., Zhang, B., & Wei, D. M. 2005, ApJ, 629, 334
Genet, F., Daigne, F., & Mochkovitch, R. 2007, MNRAS, 381, 732
Golenetskii, S., Aptekar, R., Frederiks, D., et al. 2013, GCN, 14487, 1
Kouveliotou, C., Granot, J., Racusin, J. L., et al. 2013, ApJL, 779, L1
Laskar, T., Berger, E., Zauderer, B. A., et al. 2013, ApJ, 776, 119
Lemoine, M., Li, Z., & Wang, X.-Y. 2013, MNRAS, 435, 3009
Levan, A. J., Cenko, S. B., Perley, D. A., & Tanvir, N. R. 2013, GCN, 14455, 1
Liu, R.-Y., Wang, X.-Y., & Wu, X.-F. 2013, ApJL, 773, L20
Panaitescu, A., Vestrand, W. T., & Woźniak, P. 2013, MNRAS, 436, 3106
Perley, D. A., Cenko, S. B., Corsi, A., et al. 2014, ApJ, 781, 37
Piran, T., & Nakar, E. 2010, ApJL, 718, L63
Sironi, L., & Spitkovsky, A. 2011, ApJ, 726, 75
Tam, P.-H. T., Tang, Q.-W., Hou, S.-J., Liu, R.-Y., & Wang, X.-Y. 2013, ApJL, 771, L13
Thompson, C., & Madau, P. 2000, ApJ, 538, 105
Uhm, Z. L., & Beloborodov, A. M. 2007, ApJL, 665, L93
Vestrand, W. T., Wren, J. A., Panaitescu, A., et al. 2014, Sci, 343, 38